EUCAS2025-3-LO-SC.1I

Thermo-magnetic Instabilities in MgB_2 Bulk Magnets: A Combined Experimental and Numerical Investigation

Michela Fracasso, Yiteng Xing, Pierre Bernstein, Jacques Noudem, Gianluca Ghigo, Roberto Gerbaldo, and Laura Gozzelino

***Abstract*—The ability of MgB_2 polycrystalline samples to carry strong current densities even across high-angle grain boundaries has boosted the fabrication of large bulk superconductors. However, the occurrence of thermomagnetic instabilities, such as flux jumps, compromises the use of this compound at low working temperatures. Investigating and mitigating these phenomena are then crucial for future applications, as for instance permanent bulk magnets. In this paper, starting from the experimental evidence of flux-jump occurrence in a MgB_2 disc-shaped magnet prototype, we numerically investigated this phenomenon coupling the electromagnetic equations (formulated using the magnetic vector potential) to the heat diffusion equation. This numerical approach – validated via the comparison between computed and experimental results – provided us with the evolution of the local magnetic field and temperature in correspondence to a flux-jump. Based on this information, we finally investigated possible solutions to prevent flux-jump occurrence through the improvement of the thermal exchange between the sample and the cooling stage.**

***Index Terms*—Superconducting magnets, Flux pinning, Magnetic flux density, Magnesium Diboride, Thermo-magnetic instabilities**

I. INTRODUCTION

THANKS to their high in-field performance, superconductors are promising candidates to replace the traditional solutions for applications such as bulk permanent magnets or magnetic shields. In this context, bulk superconductor-based devices also offer the additional advantage of not requiring a continuous connection to a power supply [1]. Disc- and ring-shaped permanent cryo-magnets made of cuprate superconductors [2]-[5], MgB_2 [6]-[11] and iron-based superconductors [12]-[14] have successfully been fabricated with potential applications in medical, energy, transport, particle physics fields, to name but a few. Likewise, open and semi-closed superconducting (SC) tubes have been proposed as magnetic shields [15]-[19].

Among SC materials, MgB_2 has shown great potential since its long coherence length does not prevent the flow of high current density across clean grain-boundaries, thus fostering the fabrication of large polycrystalline samples with almost isotropic and homogeneous critical current density, J_c. [20]-[23]. Moreover, MgB_2 is a rare-earth-free compound with cheap and non-toxic precursors and a working temperature (10-30 K) easily reachable using closed-cycle cryocoolers. Noteworthy, despite an irreversibility field much lower than cuprate or iron-based superconductors, trapped magnetic fields up to 6 T were predicted at 10 K in MgB_2 disc stacks [24].

On the other hand, this compound has the drawback of being affected by thermo-magnetic instabilities, such as flux-jumps, which can compromise its use at low temperatures [25]-[30]. Flux-jumps consist in abrupt readjustments of the magnetic flux lines inside the superconductor coupled with a rapid increase of its temperature, even above the transition value [31],[32]. Typically, they are triggered by a change, even a small one, of the external magnetic field or temperature that produces a magnetic flux motion inside the sample with the resulting release of a small amount of heat and the local increase of the superconductor temperature. This in turn causes a local J_c reduction generating a further flux-line motion with a consequent electric field perturbation. As a result, additional heat is released inside the sample. In such a way, due to the low heat capacity and thermal conductivity of MgB_2 [33], an iterative process begins that quickly leads to a sharp increase of the sample temperature and to the nucleation of magnetic flux avalanches. In the theoretical investigation of the flux-jump phenomena the achievement of a local adiabatic condition is usually assumed. This hypothesis can be considered fulfilled when the thermal diffusion coefficient, D_t, is much lower than the magnetic diffusion one, D_m, [34],[35] as verified at low temperature in MgB_2 [33].

Several approaches have been pursued to mitigate this phenomenon. The slower the external magnetic field/temperature variation over time, the more resilient against flux jump occurrence the sample is [36]. However, it is not always possible to have a real control on the

This work is the result of an international collaboration strengthened by the support of the European Cooperation in Science and Technology (COST) action CA19108. This work was also partially supported by I.N.F.N.- C.S.N. 5 under the experiments SAMARA and SuperMAD and by the Space It Up project funded by the Italian Space Agency, ASI, and the Ministry of University and Research, MUR, under contract n. 2024-5-E.0 - CUP n. I53D24000060005. *(Corresponding author: laura.gozzelino@polito.it).*

Michela Fracasso, Gianluca Ghigo, Roberto Gerbaldo, and Laura Gozzelino are with the Department of Applied Science and Technology, Politecnico di Torino and I.N.F.N. Sez. di Torino, Torino, 10129 Italy (e-mail: michela.fracasso@polito.it, gianluca.ghigo@polito.it, roberto.gerbaldo@polito.it, laura.gozzelino@polito.it).

Yiteng Xing, Pierre Bernstein and Jacques Noudem are with the Normandie Univ, Ensicaen, Unicaen, CNRS, CRISMAT, Caen, 14000, France. (e-mail: yiteng.xing@ensicaen.fr, pierre.bernstein@ensicaen.fr, jacques.noudem@ensicaen.fr).

field/temperature ramp rate. Aldica *et al.* [37] highlighted that the heating rate in MgB_2 growing process can affect the flux-jump occurrence. Adding additives can also influence both the magnitude and the frequency occurrence of flux jumps as found in FeTi- and graphene-doped MgB_2 bulk samples, respectively [38],[39]. Higher thermomagnetic stability was also observed in machinable MgB_2 samples fabricated with the addition of graphene instead of h-BN [40]. Furthermore, based on results achieved on other superconductors affected by the same issue [41], an improvement of the thermomagnetic stability is expected using other appropriate doping elements. Another way to hinder the iterative process giving rise to flux jumps is the improvement of the thermal exchange between the sample and the cooling sources [42]-[45].

In our previous papers, we investigated the effect of flux-jump occurrence in a MgB_2 cup-shaped shield [17],[45]. To this aim, we compared the experimental data with the outputs of a numerical analysis coupling both electromagnetic and thermal equations [40]. This numerical approach proved to be efficient in reproducing the experimental data, thus accurately predicting the decay of the shielding properties induced by thermomagnetic instability occurrence. The same model evidenced the improvement of the heat exchange between the MgB_2 shield and the cryocooler cooling stage [45] as well as the superimposition of a high-thermal-capacitance ferromagnetic shield on the SC one [18] as two possible routes to increase the thermomagnetic stability of this device.

In this paper, the same numerical model is applied to investigate the flux-jump occurrence in the magnetization process of a MgB_2 bulk disc providing a good agreement between the experimental and computed results. To describe the in-field and thermal behavior of the sample, we considered its critical current density dependence on magnetic field and temperature, as well as its thermal conductivity and specific heat values. The analysis of the temperature distribution inside the disc in the time frame of flux-jump nucleation and propagation guided us in the study of alternative layouts able to guarantee a better heat exchange with the cooling stage of the cryocooler.

The paper is organized as follows. In section II, we describe the sample fabrication process and report on the experimental procedures used for its characterization, while details on the finite-element method used for the numerical calculations are reported in section III. The comparison between the trapped field values achieved both experimentally and numerically is shown in section IV, where also the local temperature of the sample in the time interval in which a flux jump nucleates and starts propagating is investigated. Possible routes for improving the thermal stability of the samples are then proposed and compared. The main findings are finally summed up in section V.

II. Experimental Details

A. MgB_2 fabrication process and thermal properties

The MgB_2 cylindrical bulk samples were fabricated via the in-situ Spark Plasma Sintering (SPS) process. The starting materials were magnesium metal powder (99.8%, 325 mesh, Alfa Aesar) and amorphous boron powder (99%, <400 nm, PAVEZYUM Advanced Chemicals), mixed in a molar ratio of 1:2 under an argon atmosphere. A 6.2 g charge of the mixed powder was located into a tungsten carbide (WC) mold with a diameter of 20 mm and sintered using an SPS system (FCT Systeme HD25) under dynamic vacuum (10^{-3} mbar). The sintering process involved a sequential increase in temperature and pressure as follows:

i) 500 °C + 260 MPa / 15 min (powder compaction).
ii) 650 °C + 280 MPa / 20 min (synthesis).
iii) 750 °C + 300 MPa / 60 min (sintering/densification)

The final sintered bulk disc had a diameter of 20 mm, a thickness of 8 mm, and a density of 2.46 g/cm^3. The transition temperature was T_c = 38.25 K. Detailed analyses of the microstructure and J_c dependence on magnetic field and temperature are reported elsewhere [46]. The thermal conductivity and specific heat measured on a twin sample are shown in Fig. 1.

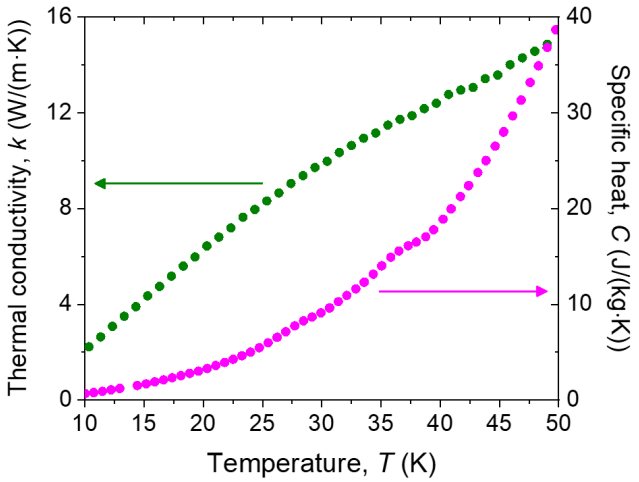

Fig. 1. Thermal conductivity (green symbols) and specific heat (magenta symbols) measured on a small twin sample grown following the same sintering procedure as the disc.

B. Measurements details

Magnetization measurements were carried out using a Physical Property Measurement System (PPMS, Quantum Design, San Diego, CA, USA). The magnetic field at the sample's top surface center was measured with a Hall probe (HE144, Asensor Technology AB, Sweden). The sample was wrapped in an Al foil to improve the thermal exchange and mounted in a brass PPMS holder, with its bottom surface in contact with a copper plate fixed using varnish to ensure good thermal contact. A schematic drawing of the experimental setup is shown in Fig. 2 (a). The magnetization process followed a field-cooling (FC) procedure. The sample was first stabilized at 45 K, a temperature above T_c. An external magnetic field was then increased up to 9 T at a rate of 0.9 T/min. Keeping the external field constant, the sample was cooled down to the target measurement temperatures (20, 15,

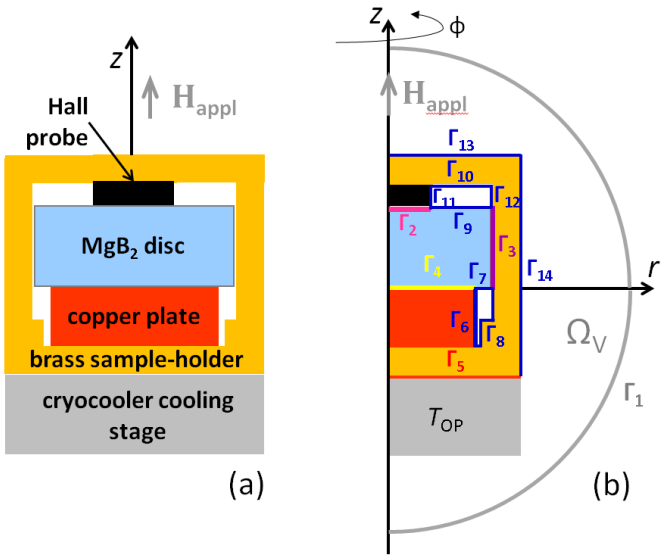

Fig. 2. (a) Schematic drawing of the experimental setup (not to scale) for the trapped field measurement. The MgB_2 disc, wrapped in an Al foil, was placed on a cooper plate and mounted in the brass PPMS holder. The external field was applied along the *z*-direction and the Hall probe oriented so as to measure the component of the magnetic flux density parallel to the applied field was positioned at the center of the sample top surface. (b) 2D axisymmetric model of the experimental set-up implemented in COMSOL. Γ_1-Γ_{14} identify domain interfaces (see main text), T_{OP} is the cooling stage temperature and Ω_v the external domain (vacuum).

and 10 K) and held at that temperature for one hour to ensure thermal stabilization. The magnetic field was then gradually reduced according to the following protocols to minimize flux jumps at each measurement temperature:

- at 20 K: 9 T → 0 T at 0.06 T/min;
- at 15 K: 9 T → 3 T at 0.06 T/min, then 3 T → 0 T at 0.015 T/min;
- at 10 K: 9 T → 4 T at 0.06 T/min, then 4 T → 0 T at 0.006 T/min.

III. Numerical Modeling

A. Electromagnetic and thermal equations

To reproduce the experimental data, the model equations have to account both for the electromagnetic and the thermal behavior of the superconductor [47]. The model was implemented by the finite element software COMSOL 6.2 Multiphysics® [48] coupling the magnetic field interface (*mf*) and the heat transfer module (*ht*).

The changes in the local value of temperature in the SC domain and sample-holder regions were calculated using the following heat diffusion equation:

$$\nabla \cdot (k(T)\nabla T) - C(T) \cdot \rho_m \cdot \frac{\partial T}{\partial t} + Q = 0$$

where $Q = \mathbf{E} \cdot \mathbf{J}$ gives the volumetric heating rate and ρ_m, k, and C are the mass density, thermal conductivity, and specific heat, respectively. The temperature dependence of the last two parameters, $k(T)$ and $C(T)$ were involved in the model via a piecewise cubic interpolation of the experimental data reported in Fig. 1.

The electromagnetic behaviour of the SC and the surroundings domains was described by Maxwell's equations formulated using the magnetic vector potential **A** [49],[50]. Taking advantage of the axial symmetry of the experimental set-up (see Fig. 2), the equations take the form:

$$E_\phi = -\frac{\partial A_\phi}{\partial t}$$

$$\mathbf{B} = -\frac{\partial A_\phi}{\partial z}\mathbf{u_r} + \frac{1}{r}\left[\frac{\partial}{\partial r}(rA_\phi)\right]\mathbf{u_z}$$

being $\mathbf{u_r}$ and $\mathbf{u_z}$ the unit vectors along the *r*- and *z*-directions, respectively.

The relationship between the local electric field and current density ($E - J$) in the SC domain was accounted for via the hyperbolic tangent function proposed in [49],[50], which is a smooth approximation of the stepwise $E - J$ behavior predicted in the critical state model. Accordingly, the electrical conductivity of the superconductor, σ_{SC}, considered in the Ampere Law's module in COMSOL was customized as follows:

$$\sigma_{SC} = \frac{1}{|E_\phi|} J_c(B,T) \cdot \tanh\left(\frac{|E_\phi|}{E_0}\right) + \sigma_{norm}$$

where σ_{norm} is the normal state conductivity, here assumed to be equal to 10^8 S/m, as proposed in [31] and E_0 is a threshold electric field that controls the sharpness of the $E - J$ function [51], set to 10^{-5} V/m in this case [45].

The magnetic field and temperature dependence of the critical current density J_c (B,T) was accounted for by fitting the experimental J_c curved reported in [46] by the equation:

$$J_c(B,T) = J_{c0}(T) \cdot \exp\left[-\left(\frac{B}{B_0(T)}\right)^{\gamma(T)}\right]$$

where the temperature dependence of the parameters J_{c0} , B_0 and γ takes the form:

$$J_{c0}(T) = \alpha_1\left[1 - \left(\frac{T}{T_c}\right)^{\alpha_2}\right]^{\alpha_3} \quad (1)$$

$$B_0(T) = \beta_1\left[1 - \left(\frac{T}{T_c}\right)^{\beta_2}\right]^{\beta_3} \quad (2)$$

$$\gamma(T) = \gamma_1 + \gamma_2 T + \gamma_3 T^2 \quad (3)$$

and α_i, β_i and γ_i (i = 1, 2, 3) are fit coefficients. Their values are summarized in table I.

The thermal equation was solved exclusively within the material domains, namely the SC, brass, copper and Hall probe regions. In contrast, the electromagnetic equations were solved in all domains, including the vacuum region (Ω_V) (see the model schematic in Fig. 2 (b)).

TABLE I
PARAMETERS EMPLOYED FOR THE ELECTROMAGNETIC MODELING OF THE MgB_2 DISC

Parameters	Description	Value
E_0	Threshold electric field	10^{-5} V/m
T_c	Critical temperature	38.25 K
σ_{norm}	Normal state conductivity	10^8 S/m
α_1	Parameter of equation (1)	$1.01 \cdot 10^{10}$ Am^{-2}
α_2	Parameter of equation (1)	1.92
α_3	Parameter of equation (1)	1.41
β_1	Parameter of equation (2)	3.20 T
β_2	Parameter of equation (2)	2.04
β_3	Parameter of equation (2)	1.39
γ_1	Parameter of equation (3)	0.021
γ_2	Parameter of equation (3)	$-9.6 \cdot 10^{-5}$ K^{-1}
γ_3	Parameter of equation (3)	1.85 K^{-2}
ρ_m	MgB_2 mass density	2.46 g/cm^3

B. Boundary conditions

During the experiment, the sample was wrapped by an aluminum foil and cooled via the tight thermal contact with the copper plate located below it (see Fig. 2(a)). A thermal contact between the sample and the brass sample-holder was also assumed through the Hall probe package and the lateral wall (Γ_2 and Γ_3 boundaries in Fig. 2(b), respectively), even though with a lower exchange coefficient.

To properly describe the interfacial heat flux density between the sample and the environment we used the boundary conditions reported below. The thermal exchange between the brass sample-holder and the cryocooler cooling stage was modelled defining the following equation on boundary Γ_5 (see Fig. 2 (b)):

$$\mathbf{u_n} \cdot (-k_{Br}(T) \cdot \nabla T) = \Psi_1 \cdot (T_{OP} - T_{brass}) \quad (4)$$

where Ψ_1 denotes the heat transfer coefficient, T_{OP} the operational temperature (corresponding to the cooling stage temperature), T_{brass} the temperature of the brass sample-holder, and k_{Br} the brass thermal conductivity. $\mathbf{u_n}$ is the unit vector perpendicular to the boundary surface.

On interface Γ_2, Γ_3 and Γ_4 traced in Fig. 2 (b), the thermal contact node was employed to model the heat transfer between the superconductor and, respectively, the Hall probe, the brass sample-holder, and the copper plate. The thermal exchange equations at these boundaries are:

Across Γ_2: $\mathbf{u_n} \cdot (-k_{Al}(T) \cdot \nabla T) = \Psi_2 \cdot (T_{Hall\ Probe} - T_{SC})$ (5)

Across Γ_3: $\mathbf{u_n} \cdot (-k_{Al}(T) \cdot \nabla T) = \Psi_3 \cdot (T_{brass} - T_{SC})$ (6)

Across Γ_4: $\mathbf{u_n} \cdot (-k_{Al}(T) \cdot \nabla T) = \Psi_1 \cdot (T_{copper} - T_{SC})$ (7)

where k_{Al} is the aluminium thermal conductivity and $T_{\text{Hall probe}}$, T_{copper} and T_{SC} are the temperature of the Hall probe package, copper plate and superconductor, respectively. To take into account the different thermal coupling across the different contact surface, we assumed $\Psi_2 = \Psi_1/20$ and $\Psi_3 = \Psi_1/100$. Ψ_1 evaluated through an iterative procedure is 10000 W/(m^2 K). No thermal exchange was assumed across the interfaces Γ_6 – Γ_{14}.

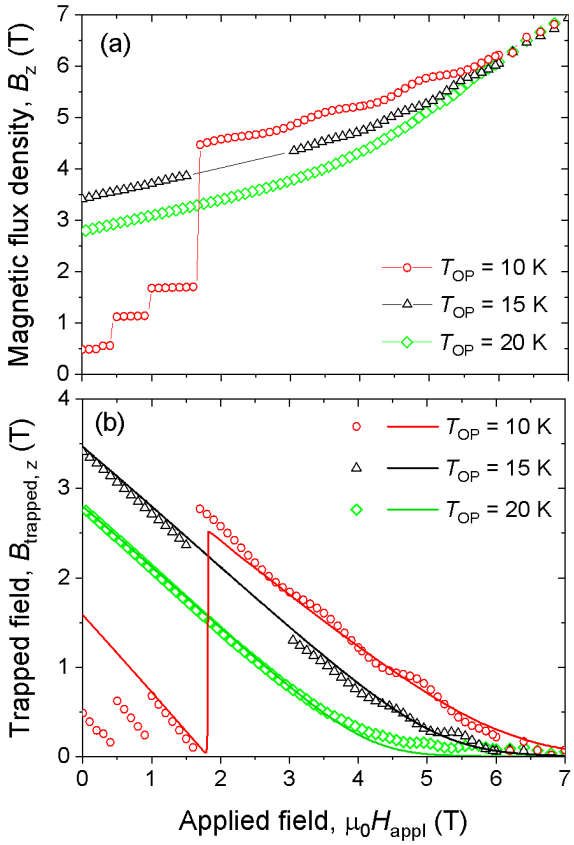

Fig. 3. (a) Magnetic flux density measured at the center of the top surface of the disc. (b) Trapped field values measured (symbols) and calculated (lines) at the same position as in panel (a).

The source term for the applied magnetic field, H_{appl}, was considered through the boundary condition on surface Γ_1: at a large distance from the disc, the magnetic flux density was assumed to be constant and equal to the applied field.

IV. RESULTS AND DISCUSSION

Fig. 3(a) shows the values of the magnetic flux density measured at T_{OP} = 10, 15 and 20 K as the applied field was reduced. No flux-jumps were recorded at 15 K and 20 K and a remnant magnetic flux density of 3.4 T and 2.8 T was achieved, respectively, after field zeroing. These results are only slightly lower than the highest trapped field values obtained on MgB_2 discs of similar size [52], [53]. This difference can be attributed both to geometric factors (for example a slightly larger radius in the case of the discs shown in [53]) and to the different growth techniques and precursor's grain size. Conversely, at 10 K, some flux jumps occurred when the applied field decreased below 1.7 T.

Fig. 3(b) compares the measured and computed values of the trapped field, $B_{\text{trapped,z}}$, defined as the difference between the magnetic flux density B_z and the applied field, $\mu_0 H_{appl}$.

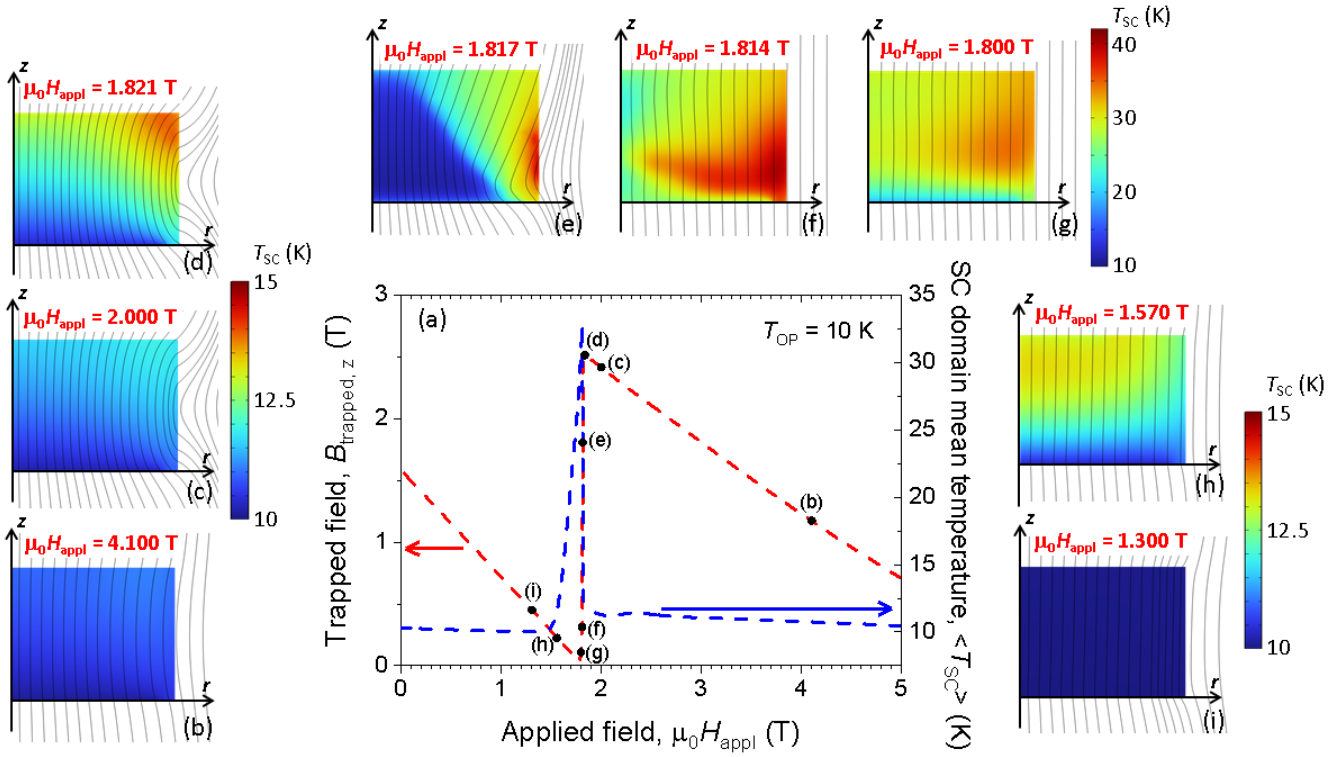

Fig. 4. (a) Evolution of the trapped field calculated at the center of the top surface of the disc (red curve) and of the SC disc average temperature (blue curve) while the applied field is decreasing. Dots (b) – (i) identify the applied field values at which the maps reported in the corresponding panels (b)-(i) were extracted. (b)-(i) Magnetic flux line and temperature distributions (color maps) in the MgB_2 disc at the applied magnetic fields highlighted with dots in panel (a). Panels (b)-(d) share the same color bar. The same for panels (e)-(g) and panels (h)-(i).

Note that after the applied field removal the remnant flux density coincides with the trapped field. Clearly, at 15 and 20 K there is a remarkable agreement between the experimental and modelling results. At 10 K, the calculated curve replicates very well the occurrence of the first flux-jump at 1.7 T, but fails to reproduce the subsequent ones, indicating that the layout of the experimental set-up introduced in the model still needs further refinements. Despite this discrepancy, the numerical computation, predicting the variation of the temperature distribution inside the sample as the applied field decreases, can be a guide for designing experimental setup adjustments able to improve the thermal exchange between the sample and the cooling source.

The temperature distribution inside the disc calculated at T_{OP} = 10 K as the applied field decreases is reported in panels (b) – (i) of Fig. 4 and correlated to the value of the trapped field plotted in panel (a). The average temperature of the superconductor – calculated applying the *Mean Probe* function in Comsol to the variable T_{SC} of the SC domain – is shown in panel (a), as well. As can be seen from the temperature color maps, when the flux-jump occurs the temperature of the disc locally exceeds 40 K causing a partial transition of the sample to the normal state. Concurrently, the average temperature of the disc rises above 32 K and the magnetic flux lines take an almost regular spacing and a direction parallel to the applied field direction indicating an homogenous penetration of the magnetic field inside the sample and a zero trapped field value. The heat is then removed from the sample but its ability to work as a permanent magnet is compromised (it can be restored only by repeating the whole magnetization process).

Figs. 4 (e),(f) highlight that the sample overheating, which gives rise to the flux-jump, is triggered by a hot spot developing in correspondence to the lateral surface of the disc.

Based on this evidence, we first simulated what could be expected if the thermal contact between the lateral surface of the sample and the brass sample-holder was improved. To this aim, we modified (6) assuming a heat transfer coefficient Ψ_1 across interface Γ_3 instead of Ψ_3. Following this adjustment, a flux-jump of amplitude similar to that occurred in the previous configuration still arises, although at an applied field 0.25 T lower than before (Fig. 5).

Therefore, considering that before the flux-jump nucleation a heating was already detected at the top outer region of the sample (panel (d) of Fig. 4), a second attempt was done also assuming that the area delimited by the interfaces Γ_9 – Γ_{10} – Γ_{11} – Γ_{12} (Fig. 2 (b)) was completely filled with an indium ring, which in turn was assumed to be in good thermal contact with the brass sample-holder. Accordingly, the equation governing the thermal exchange across the interface Γ_9 becomes:

$$\mathbf{u_n} \cdot (-k_{Al}(T) \cdot \nabla T) = \Psi_1 \cdot (T_{indium} - T_{SC}) \qquad (8)$$

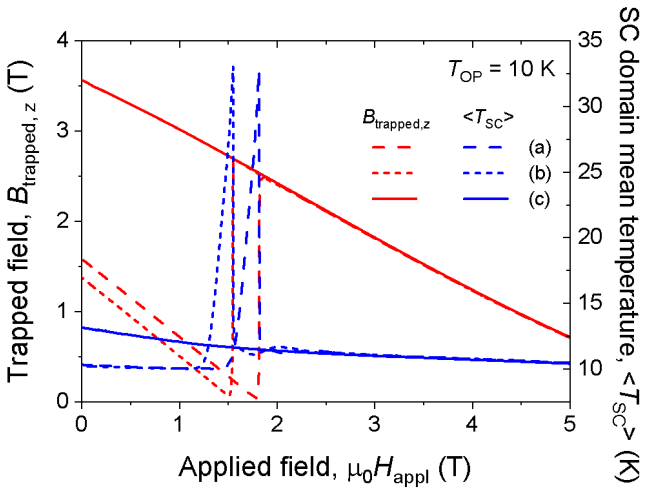

Fig. 5. Trapped field (red curves) and SC disc mean temperature (blue curves) calculated assuming (a) the same layout as in the experiment (see Fig. 2 (b) and the main text in Section III.B), (b) a heat transfer coefficient Ψ_1 across interface Γ_3 instead of Ψ_3 (see Fig. 2 (b) and equation (6)) and (c) a heat transfer coefficient Ψ_1 across interface Γ_3 instead of Ψ_3 and an indium ring totally filling the area delimited by the interfaces $\Gamma_9 - \Gamma_{10} - \Gamma_{11} - \Gamma_{12}$ (see Fig. 2 (b) and equation (8)).

As shown in Fig. 5 (curves labelled (c)), this further improvement in heat exchange totally prevents the appearance of flux jumps and the computation predicts a maximum trapped field greater than 3.5 T.

V. CONCLUSIONS

In this work, we investigated the flux-jump occurrence in a prototype of MgB_2 disc-shaped permanent magnet. To this aim, the experimental characterization was supported by a numerical model coupling electromagnetic equations based on the **A**-formulation to the heat diffusion equation in order to gain a comprehensive understanding of this phenomenon.

The disc was magnetized in the normal state, then after being cooled down to the working temperature the external magnetic field was removed. A trapped field of 2.8 and 3.4 T was measured at 20 and 15 K, respectively, in correspondence of the center of the sample top surface, while at 10 K a multiple flux-jump occurrence markedly compromised the maximum achievable trapped field. The comparison with the computed $B_{trapped,z}$ curves evidences a good agreement at 20 and 15 K. At 10 K, the calculated curve well reproduces the first jump occurring in the experimental curve but cannot predict the smaller jumps at lower applied fields.

Nevertheless, the calculation of the temperature distribution inside the disc guided us in studying possible improvements in the heat exchange between the sample and the cooling system to mitigate the thermal instabilities. The numerical analysis shows that a good thermal exchange on only one of the two base surfaces and on the lateral surface is not sufficient to guarantee the thermal stability. Conversely, an additional adequate heat transfer through at least part of the second base surface could be enough to prevent flux-jump occurrence.

Additional refinements of the model are still underway to achieve more accurate predictions and reach a better agreement with the experimental results. At the same time, we are planning further experiments with a new setup modified according to the computation outputs in order to guarantee an improved heat exchange between the sample and cryocooler.

ACKNOWLEDGMENT

M.F. and L.G. thank Fedor Gömöry and Mykola Solovyov for the fruitful discussions on numerical modeling implementation.

REFERENCES

[1] J. H Durrell *et al.*, “Bulk superconductors: a roadmap to applications” *Supercond. Sci. Technol.* vol. 31, no. 10, Oct. 2018, Art. no. 103501, doi: 10.1088/1361-6668/aad7ce.

[2] T. Nakamura *et al.*, “Development of a superconducting bulk magnet for NMR and MRI” *J. Magn. Reson.* Vol. 259, pp 68-75, Oct. 2015, doi: 10.1016/j.jmr.2015.07.012.

[3] D. Zhou *et al.*, “A portable magnetic field of >3 T generated by the flux jump assisted, pulsed field magnetization of bulk superconductors featured” *Appl. Phys. Lett.* vol. 110, no. 6, Feb. 2017, Art. no. 062601, doi: 10.1063/1.4973991.

[4] Z. Chen *et al.*, “Recent progress in high-temperature superconducting undulators” *Superconductivity*, vol. 12, Dec. 2024, Art. no. 100134, doi: 10.1016/j.supcon.2024.100134.

[5] Q. Nouailhetas *et al.*, “Characterisation of large-sized REBaCuO bulks for application in flux modulation machines.” *Materials*, vol. 17, Aug. 2024, Art. no. 3827, doi: 10.3390/ma17153827.

[6] A. Yamamoto, A. Ishihara, M. Tomita, K. Kishio “Permanent magnet with MgB_2 bulk superconductor” *Appl. Phys. Lett.* vol. 21, no. 3, July 2014; Art. no. 032601, doi: 10.1063/1.4890724.

[7] M. Muralidhar, “Development of MgB_2 superconducting super-magnets: its utilization towards sustainable development goals” in High-T_c Superconducting Technology, 1st ed., Jenny Stanford Publishing, 2021 195-232.

[8] Y Xing *et al.*, “Very strong levitation force and stability achieved with a large MgB_2 superconductor disc” *Supercond. Sci. Technol.*, vol. 37, Jan. 2024, Art. no. 02LT01, doi: 10.1088/1361-6668/ad1aea.

[9] M. Fracasso *et al.*, "Comparison of the field trapping ability of MgB_2 and hybrid disc-shaped layouts," *Materials*, vol. 17, no. 5, Mar 2024, Art no. 1201, doi: 10.3390/ma17051201.

[10] T. Kii, M. Tomita and T. Akasaka, "Generation of periodic magnetic field using bulk MgB_2," *IEEE Trans. Appl. Supercond*., vol. 34, no. 3, May 2024, Art no. 4101604, doi: 10.1109/TASC.2024.3356503.

[11] T. Prikhna, V. Sokolovsky, and V, Moshchil "Bulk MgB_2 superconducting materials: technology, properties,” and applications," *Materials*, vol. 17, no. 11, June 2024, Art no. 2787, doi: 10.3390/ma17112787.

[12] J. D. Weiss, A. Yamamoto, A. A. Polyanskii, R.B. Richardson, D. C. Larbalestier, and E. E. Hellstrom, “Demonstration of an iron-pnictide bulk superconducting magnet capable of trapping over 1 T” *Supercond. Sci. Technol.*, vol. 28, no. 11, Nov. 2015, Art. no. 112001, doi: 10.1088/0953-2048/28/11/112001.

[13] A. Yamamoto, S. Tokuta, S., A. Ishii, A. Yamanaka, Y. Shimada and M. D. Ainslie, “Superstrength permanent magnets with iron-based superconductors by data- and researcher-driven process design” *NPG Asia Mater* vol. 16, July 2024, Art. no. 29, doi: 10.1038/s41427-024-00549-5.

[14] T. Tamegai, W. X. Wu, C. Yu and R. Sakagami, "Bulk 122-type iron-based superconductors sintered under high pressure," *IEEE Trans. Appl. Supercond.*, vol. 34, no. 3, May 2024, Art no. 7300705, doi: 10.1109/TASC.2023.3347683.

[15] L. Wéra, J. -F. Fagnard, D. K. Namburi, Y. Shi, B. Vanderheyden and P. Vanderbemden, "Magnetic shielding above 1 T at 20 K with bulk, large grain YBCO tubes made by buffer-aided top seeded melt growth," *IEEE Trans. Appl. Supercond.*, vol. 27, no. 4, June 2017, Art no. 6800305, doi: 10.1109/TASC.2016.2633301.

[16] G. Giunchi, D. Barna, H. Bajas, K. Brunner, A. Német and C. Petrone, "Creep and relaxation phenomena in a long MgB_2 tube subjected to transverse magnetic field, at 4.2 K," *IEEE Trans. Appl. Supercond.*, vol. 28, no. 4, Mar. 2018, Art no. 6801705, doi: 10.1109/TASC.2018.2816101.

[17] L. Gozzelino *et al.*, "High magnetic shielding properties of an MgB_2 cup obtained by machining a spark plasma-sintered bulk cylinder," *Supercond. Sci. Technol.*, vol. 33, no. 4, Apr. 2020, Art. no. 044018, doi: 10.1088/1361-6668/ab7846.

[18] N. Rotheudt, M. Fracasso, P. Vanderbemden, and L. Gozzelino, "Superconductor-based passive shielding and screening systems," *Supercond. Sci. Technol.,* vol. 38, no. 4, Apr. 2025, Art. no. 043002, doi: 10.1088/1361-6668/adb7cc.

[19] CAN Superconductors, (available at: https://www.can-superconductors.com/hts-bulks-and-materials/bi-2223-magnetic-shields/) (last access October 13th, 2025).

[20] T. Naito, T. Sasaki, and H, Fujishiro, "Trapped magnetic field and vortex pinning properties of MgB_2 superconducting bulk fabricated by a capsule method," *Supercond. Sci. Technol.*, vol. 25, no. 9, Sep. 2012, Art. no. 095012, doi: 10.1088/0953-2048/25/9/095012.

[21] A. Ishihara, T. Akasaka, M. Tomita, and K. Kishio, "Superior homogeneity of trapped magnetic," *Supercond. Sci. Technol.,* vol. 30, no. 3, Mar. 2017, Art. no. 035006, doi: 10.1088/1361-6668/30/3/035006.

[22] A. G. Bhagurkar et al., "A trapped magnetic field of 3 T in homogeneous, bulk MgB_2 superconductors fabricated by a modified precursor infiltration and growth process," *Supercond. Sci. Technol.,* vol. 29, no. 3, Mar. 2016, Art. no. 035008, doi: 10.1088/0953-2048/29/3/035008.

[23] N. Ikeda, M. Ainslie, R. Tanaka, and A. Yamamoto, "A comparative study of experimental and simulated trapped magnetic field of MgB_2 bulks prepared by the magnesium vapor transport process," *IEEE Trans. Appl. Supercond.*, vol. 33, no. 5, Aug. 2023, Art no. 6800505, doi: 10.1109/TASC.2023.3253070.

[24] M. Miryala, T. Naito, M. Jirsa, and J. Noudem, "Nanostructured compact bulk MgB_2 cryo-magnets with record-high critical currents and trapped magnetic fields" *Sci. Rep.*, vol. 15, Oct. 2025, Art. no. 36308, doi: 10.1038/s41598-025-97195-w.

[25] C. Romero-Salazar, F. Morales, R. Escudero, A. Durán and O. A. Hernández-Flores, "Flux jumps in hot-isostatic pressed bulk MgB_2 superconductors: experiment and theory," *Phys. Rev. B,* vol. 76, no. 10, Sep. 2007, Art. no. 104521, doi: 10.1103/PhysRevB.76.104521.

[26] G. Giunchi, D. Turrioni, V. Kashikhin, H. Nguyen, and E. Barzi, "Feasibility study of a MgB_2 superconducting magnetic cloak," *IEEE Trans. Appl. Supercond.*, vol. 26, no. 3, Apr. 2016, Art no. 8801005, doi: 10.1109/TASC.2016.2539261.

[27] K. Berger *et al.*, "High magnetic field generated by bulk MgB_2 prepared by Spark Plasma Sintering," *IEEE Trans. Appl. Supercond.*, vol. 26, no. 3, Apr. 2016, Art no. 6801005, doi: 10.1109/TASC.2016.2537143.

[28] T Qureishy *et al.*, " Dendritic flux avalanches in a superconducting MgB_2 tape," *Supercond. Sci. Technol.*, vol. 30, no. 12, Dec. 2017, Art no. 125005, doi: 10.1088/1361-6668/aa9244.

[29] T. Prikhna *et al.*, "Trapped fields of hot-pressed MgB_2 for applications in liquid hydrogen," *IEEE Trans. Appl. Supercond.*, vol. 33, no. 5, Aug. 2023, Art no. 6801105, doi: 10.1109/TASC.2023.3248531.

[30] G. J. Ruan *et al.*, "Unusual flux jump behaviors and pinning mechanism of MgB_2 bulks at low temperature" *Mater. Today Commun.*, vol. 46, June 2025, Art. no. 112471, doi: 10.1016/j.mtcomm.2025.112471.

[31] J. Xia, M. Li, and Y. Zhou, "Numerical investigations on the characteristics of thermomagnetic instability in MgB_2 bulks," *Supercond. Sci. Technol.*, vol. 30, no. 7, July 2016, Art. no. 075004, doi: 10.1088/1361-6668/aa73b3.

[32] Z. Jing, "Coupled multiphysics modeling of the thermal-magnetic-mechanical instability behavior in bulk superconductors during pulsed field magnetization" *Supercond. Sci. Technol.*, vol. 35, no. 5, May 2022, Art. no. 054006, doi: 10.1088/1361-6668/ac5be8.

[33] V. Chabanenko *et al.*, "Flux jumps and H-T diagram of instability for MgB_2" *J. Low Temp. Phys.*, vol. 130, pp. 175-191, Feb. 2003, doi: 10.1023/A:1022236117354

[34] G. R. Mints and A. L. Rakhmanov "Critical state stability in type-II superconductors and superconducting-normal-metal composites", *Rev. Mod. Phys.*, vol. 53, no. 3, pp. 551–592, July 1981, doi: 10.1103/RevModPhys.53.551.

[35] G. R. Mints, "Flux creep and flux jumping," *Phys. Rev. B*, vol. 53, no. 18, pp. 12311-12317, May 1996, doi: 10.1103/PhysRevB.53.12311.

[36] D. A. Moseley, D. P. Wilkinson, T. Mousavi, A. R. Dennis, S. Speller and J. H. Durrell, "A new MgB_2 bulk ring fabrication technique for use in magnetic shielding or bench-top NMR systems," *Supercond. Sci. Technol.*, vol. 35, no. 8, Aug. 2022, Art. no. 085003, doi: 10.1088/1361-6668/ac7587.

[37] G. Aldica, M. Burdusel, S. Popa, M. Enculescu, I. Pasuk, and P. Badica, "The influence of heating rate on superconducting characteristics of MgB_2 obtained by spark plasma sintering technique," *Physica C*, vol. 519, pp. 184-189, Dec. 2015, doi: 10.1016/j.physc.2015.10.004.

[38] H.B. Lee, G.C. Kim, Y.C. Kim, and D. Ahmad, "Flux jump behaviors and mechanism of FeTi doped MgB_2 at 5K," *Physica C*, vol. 515, pp. 31-35, Aug. 2015, doi: 10.1016/j.physc.2015.05.002.

[39] K. Yokoyama et al., "Investigation of flux jumps during pulsed field magnetization in graphene-added MgB_2 bulks," *J. Phys.: Conf. Ser.*, vol. 1559, 2019, Art. no. 012080, doi: 10.1088/1742-6596/1559/1/012080.

[40] M. Burdusel, G. V. Aldica, I. Pasuk, M. A. Grigoroscuta, A. Kuncser, P. Badica, "Trapped magnetic field of MgB_2 machinable disks with different additives," *J Supercond Nov Magn*, vol. 38, July 2025, Art. no. 179, doi: 10.1007/s10948-025-07002-w.

[41] X. Xu, P. Li, A. V. Zlobin and X. Peng, "Improvement of stability of Nb_3Sn superconductors by introducing high specific heat substances," *Supercond. Sci. Technol.,* vol. 31, no. 3, Mar. 2018, Art. no. 03LT02, doi: 10.1088/1361-6668/aaa5de.

[42] F Colauto *et al.*, "Mapping flux avalanches in MgB_2 films—equivalence between magneto-optical imaging and magnetic measurements," *Supercond. Sci. Technol.*, vol. 20, no. 8, pp. L48-L50, Aug. 2007, doi: 10.1088/0953-2048/20/8/L02.

[43] D. A. Moseley *et al.*, "Improved pulsed field magnetisation in MgB_2 trapped-field magnets," *Supercond. Sci. Technol.*, vol. 34, no. 8, Aug. 2021, Art. no. 085018, doi: 10.1088/1361-6668/ac0951.

[44] J. Longji Dadiel et al., "Field-trapping performance of drilled MgB_2 bulk superconductor embedded with Bi-In-Sn alloy and Al-rod using pulse-field magnetization processes," *IEEE Trans. Appl. Supercond.*, vol. 32, no. 4, Apr. 2022, Art no. 3800106, doi: 0.1109/TASC.2022.3151032.

[45] M. Fracasso *et al.*, "Numerical study on flux-jump occurrence in a cup shaped MgB_2 bulk for magnetic shielding applications," *Supercond. Sci. Technol.*, vol. 36, no. 4, Apr. 2023, Art. No. 044001, doi: 10.1088/1361-6668/acbac5.

[46] Y. Xing, P. Bernstein, M. Miryala, and J. G. Noudem "High critical current density of nanostructured MgB_2 bulk superconductor densified by spark plasma sintering," *Nanomaterials*, vol. 12, no. 15, July 2022, Art. no. 2583, doi: 10.3390/nano12152583.

[47] M. Ainslie, and H. Fujishiro, *Numerical Modelling of Bulk Superconductor Magnetisation.* Bristol, UK: IOP Publishing, 2019, pp. 3-1 – 3-17.

[48] (Available at: www.comsol.com/).

[49] F Gömöry, M Vojenčiak, E Pardo, M Solovyov and J Šouc, "AC losses in coated conductors," *Supercond. Sci. Technol.*, vol. 23, no. 3, Mar. 2010, Art. no. 034012, doi: 10.1088/0953-2048/23/3/034012.

[50] L. Gozzelino *et al.*, "Screening of magnetic fields by superconducting and hybrid shields with a circular cross-section," *Supercond. Sci. Technol.*, vol. 35, no. 4, Apr. 2022, Art. no. 044002, doi: 10.1088/1361-6668/ac4ad0.

[51] M. Solovyov and F. Gömöry, "A–V formulation for numerical modelling of superconductor magnetization in true 3D geometry," *Supercond. Sci. Technol.*, vol. 32, no. 9, Sep. 2018, Art. no. 044018, doi: 10.1088/1361-6668/ab3a85.

[52] G. Fuchs *et al.*, "High trapped fields in bulk MgB_2 prepared by hot-pressing of ball-milled precursor powder," *Supercond. Sci. Technol.*, vol. 26, no. 12, Dec. 2013, Art. No. 122002, doi: 10.1088/0953-2048/26/12/122002.

[53] S. Sugino, A. Yamamoto, J. Shimoyama, and K. Kishio, "Enhanced trapped field in MgB_2 bulk magnets by tuning grain boundary pinning through milling," *Supercond. Sci. Technol*., vol. 28, no. 5, May 2015, Art. No. 055016, doi: 10.1088/0953-2048/28/5/055016.